Assimilation Behavior of Quasi-particle Comprising High Alumina Pisolitic Ore

Ji-Won JEON,[1] Sung-Wan KIM,[2] In-Kook SUH[2] and Sung-Mo JUNG[1]*

1) Graduate Institute of Ferrous Technology (GIFT), POSTECH, Cheongam-ro 77, Pohang, 790-784 Korea.
2) Resource Research Group, POSLAB, POSCO, Donghaean-ro 6261, Pohang, 790-300 Korea.

This study aims to utilize the high Al_2O_3 pisolitic ore in sintering process by designing the quasi-particle where the pisolitic ore is used as nuclei and ultra-fine hematite and magnetite ores are employed as adhering fines. The assimilation behavior between nuclei and adhering fines was investigated through microstructure analysis and it was correlated to sinter quality. When ultra-fine hematite ore was used as adhering fines, the low viscous melt of $CaO \cdot Fe_2O_3$ was formed in the assimilation. Since this results in the low extent of Al_2O_3 localization and the porous structure, the detrimental effect of Al_2O_3 on the strength was not fully controlled. On the other hand, for the ultra-fine magnetite ore, $3CaO \cdot Fe_2O_3 \cdot 3SiO_2$ melt with high viscosity was predominantly participated in the assimilation. The assimilation was suppressed by the formation of 'interfacial layer'. Due to the dense structure and high extent of Al_2O_3 localization, the detrimental effect of Al_2O_3 on strength was reasonably controlled. The quasi-particle comprising high Al_2O_3 pisolitic ore and ultra-fine magnetite ore showed the equivalent sinter quality to the quasi-particle sample consisting of nuclei of dense hematite and adhering fines of ultra-fine hematite resulting in the high sinter quality.

KEY WORDS: high Al_2O_3 pisolitic ore; quasi-particle; assimilation; primary melt; melt viscosity.

1. Introduction

Outstanding change in ironmaking area of global steel industry is ascribed to the depletion of high quality iron ore resources and to the increasing proportions of gangue materials in raw materials. In particular, the loss on ignition (LOI) and the Al_2O_3 content of iron ores are expected to gradually increase.[1,2] Under these circumstances, extensive use of low quality iron ores such as high Al_2O_3 pisolitic ore is unavoidable in ironmaking process.

There have been several researches concerning the adverse effects of pisolitic ore and Al_2O_3 content on sinter quality. It is well known that pisolitic ores have detrimental influence on sinter productivity due to its low bulk density and poor agglomeration behavior. In addition, the porous structure of sintered pisolitic ore has adverse effect on sinter strength, which is resulted from the thermal decomposition of high combined water in the ores during sintering.[3–5] On the other hand, an increase of Al_2O_3 content in sinter mix results in the increase of the formation temperature and viscosity of melt. It deteriorates sinter quality such as strength and reduction degradation characteristics (RDI), which would cause some problems with permeability during the reduction in the blast furnace.[1,6,7] To control the detrimental effect of Al_2O_3 on the sintering process, Lu et al.[2] have suggested several solutions: (1) addition of magnetite, MgO and CaO for neutralization of Al_2O_3 effect, (2) dilution of Al_2O_3 by adding high reactive ores, (3) localization of Al_2O_3 by selective granulation, (4) optimization of raw materials and sintering process. Among the above solutions, the localization of Al_2O_3 might be feasible by employing quasi-particle concept.

With the intention of overcoming the declining quality of iron ore resources, the concept of quasi-particle has been introduced to utilize low quality iron ore in sintering process.[1,8,9] Optimal design of quasi-particle structure would minimize the disadvantages of low quality ores, which can maintain and improve the sinter quality. For example, Kim et al.[1] found that the productivity and quality of sinter were improved without increasing the Al_2O_3 content in sinter by segregating high Al_2O_3 pisolitic ore in the center of quasi-particle and by coating its surface with ultra-fine iron ore. The essence of quasi-particle design is to control the assimilation behavior because it has large influence on sinter quality such as strength and reducibility.[10]

The present study aims to utilize the high Al_2O_3 pisolitic ore in sintering process by designing the quasi-particle where the pisolitic ore is used as nuclei and ultra-fine hematite and magnetite ores are employed as adhering fines. **Figure 1** shows the concept of quasi-particle design employed in the present study. The assimilation behavior between nuclei and adhering fines was investigated through microstructure analysis. Depending on the assimilation characteristics of quasi-particle, the high content of Al_2O_3 may be localized in certain region and the adverse effects of Al_2O_3
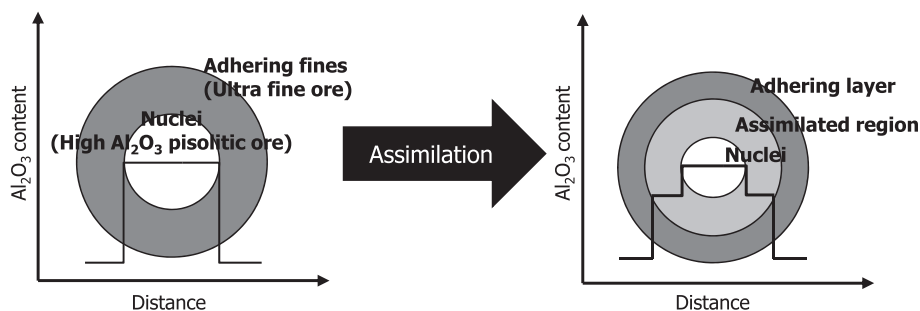
Fig. 1. Concept of quasi-particle employed in the present study.

can be suppressed. In addition, small scale sintering test was performed to correlate the assimilation behavior with sinter quality such as strength and reducibility.

2. Experimental

2.1. Materials Preparation

Table 1 shows the chemical compositions of iron ores used in the present study. Four kinds of iron ores were used for the preparation of quasi-particles. High Al_2O_3 pisolitic ore (Ore A) and dense hematite ore (Ore C) were adopted as nuclei and ultra-fine hematite (Ore N) and magnetite (Ore J) ores were used as adhering fines of the quasi-particles. Each ore was sieved to 4–5 mm for nuclei and under 100 μm for adhering fines. The quasi-particles were granulated with 50% nuclei and 50% adhering fines on the weight basis of ores. $CaCO_3$ was added to adhering fines to have the CaO/Ore value of 0.1 in the final sample composition. **Table 2** shows the chemical compositions of prepared quasi-particle samples. Experiments and analyses were performed focusing on the quasi-particles comprising high Al_2O_3 pisolitic ore A (A-N and A-J). The quasi-particle samples with dense hematite ore C (C-N and C-J) were also prepared for the sake of comparison. **Figure 2** shows the typical structure of high Al_2O_3 pisolitic ore (Ore A). It was comprised of hematite in the core and goethite surrounding it. The Si was concentrated in the core region of hematite, while Al was concentrated in the surrounding region of goethite.

In order to determine the thermal characteristics of the ores used as nuclei, loss on ignition (LOI) was measured in accordance with ASTM-D 7348. Firstly, the ores were pulverized and sieved to under 250 μm and dried for 2 hrs at 110°C. They were then heated to 950°C at a heating rate of 8°C/min and held for 2 hrs in Ar atmosphere. As a result, high Al_2O_3 pisolitic ore A showed higher LOI value compared with dense hematite ore C, which is due to the high content of combined water contained in the ore. This is because the goethite region of the ore becomes porous after dehydration.

2.2. Assimilation Degree Analysis

To investigate the assimilation behavior of quasi-particle samples, assimilation degree was evaluated by the following method.[5] About 30 g of granulated quasi-particles were first charged into a nickel crucible (35 mm in diameter, 40 mm in height). A vertical electrical resistance furnace equipped with automated sample loading system was employed and

Table 1. Chemical compositions of iron ores used in the present study (mass%).

Iron Ore		Total Fe	FeO	Al_2O_3	SiO_2	CaO	LOI	Phase
Nuclei	A	56.73	1.49	3.16	5.22	0.047	8.13	Fe_2O_3/ $FeO(OH)$
	C	64.71	0.69	1.35	2.10	0.021	1.98	Fe_2O_3
Adhering fines	N	68.07	0.64	0.47	1.07	0.021	–	Fe_2O_3
	J	68.53	27.07	0.043	1.77	0.091	–	Fe_3O_4

Table 2. Chemical compositions of prepared quasi-particle samples (mass%).

Sample	Total Fe	FeO	Al_2O_3	SiO_2	CaO
A-N	62.4	1.1	1.82	3.15	10
A-J	62.6	14.3	1.60	3.50	10
C-N	66.4	0.7	0.91	1.59	10
C-J	66.6	13.9	0.70	1.94	10

the quasi-particle samples were sintered by controlling the sample position inside the furnace maintained at 1 400°C. The samples were pre-heated at 1 100°C for 3 min, and then shifted to the zone of 1 400°C for 2 min in air stream. Subsequently, the sample was removed from the furnace for cooling. After cooling, the samples were mounted in resin and cut above 5 mm from the bottom of the crucible. Finally, it was polished to 1 μm level with diamond suspension. Due to the porous characteristics of the sample, the second mounting was done on the sample surface for clear observation.

The assimilation degree was evaluated by applying image analysis on the cross-section of the samples. As shown in **Fig. 3**, the areas of void and residual ores were distinguished and calculated by counting the number of pixels corresponding to each area. Based on the area measurement data, the area of sintered sample was calculated from the difference between total sample area and void fraction. Then the assimilation degree was determined by the following equation:

$$\text{Assimilation degree}(\%) = \left(1 - \frac{\text{area of residual ores}}{\text{area of sintered sample}}\right) \times 100$$

.... (1)

2.3. Microstructure Analysis

Backscattered electron imaging and EPMA mapping were performed for microstructure observation and EPMA sweep-

ing area analysis was conducted for further investigation on phase compositions focusing on a single quasi-particle to understand the assimilation characteristics of the samples.

Figure 4 describes the EPMA sweeping area analysis method. Since the microstructure of sinter has great inhomo-

geneity even in macroscopic observation, it is difficult to obtain the representative information of sinter sample. In this respect, EPMA sweeping area analysis might be an effective method because it targets wider area of sample.[11,12] For the quantification of Fe_2O_3, Al_2O_3, SiO_2 and CaO, the beam of 15 kV and 50 nA was employed and high purity standard materials of Fe_2O_3 (99.9%), $CaSiO_3$ (99.9%) and $CaAl_2O_5$ (99.9%) were used for the calibration of each oxide. An imaginary 20×20 grid structure was constructed on a sintered quasi-particle including the areas of nuclei and adhering fines. Each cross line of grid structure represents a quantitative measuring point. Due to the porous structure of sintered sample, only the quantification data of higher than 95% were collected in terms of total mass% of measured oxides.

2.4. Small Scale Sintering Test

Small scale sintering test for quasi-particle sample was performed employing an image gold furnace. Quasi-particle samples (300 g) containing 3 mass% of coke breeze were prepared and charged into a mullite crucible (70 mm in diameter, 95 mm in height). Then it was heated to 750°C for 10 min in N_2 atmosphere. After reaching 750°C, pre-heated air of 1 000°C was introduced into the sample layer. After introducing air for 1 min, the furnace was turned off and the samples were sintered by heat generated from the combustion of coke breeze. The sintering temperature was assumed to be approximately constant because each quasi-particle
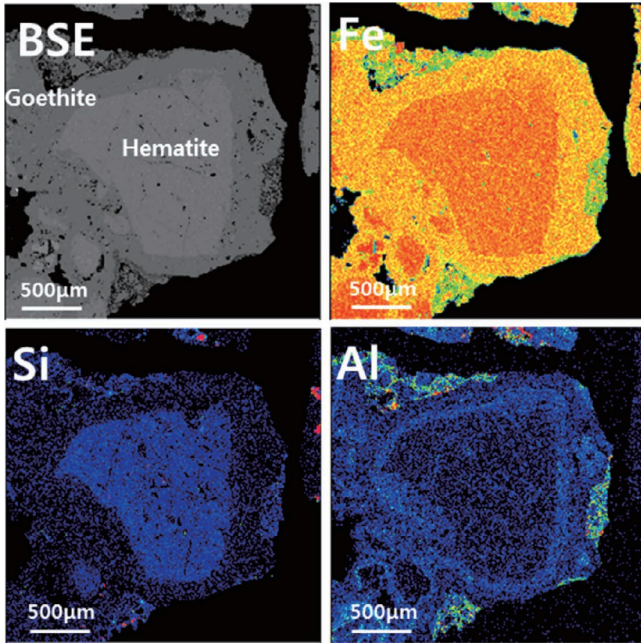

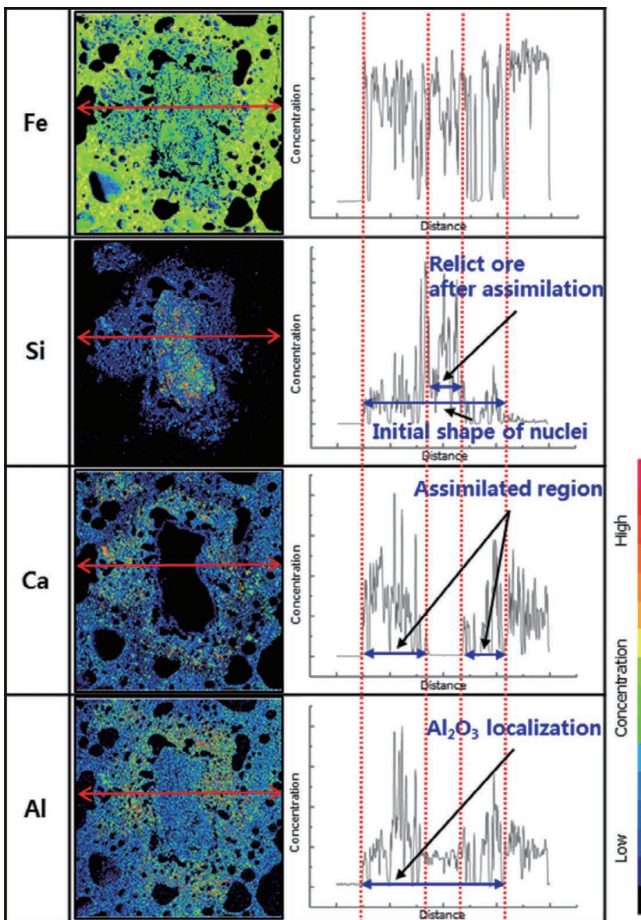**Fig. 2.** Typical structure of high Al_2O_3 pisolitic ore (Ore A).

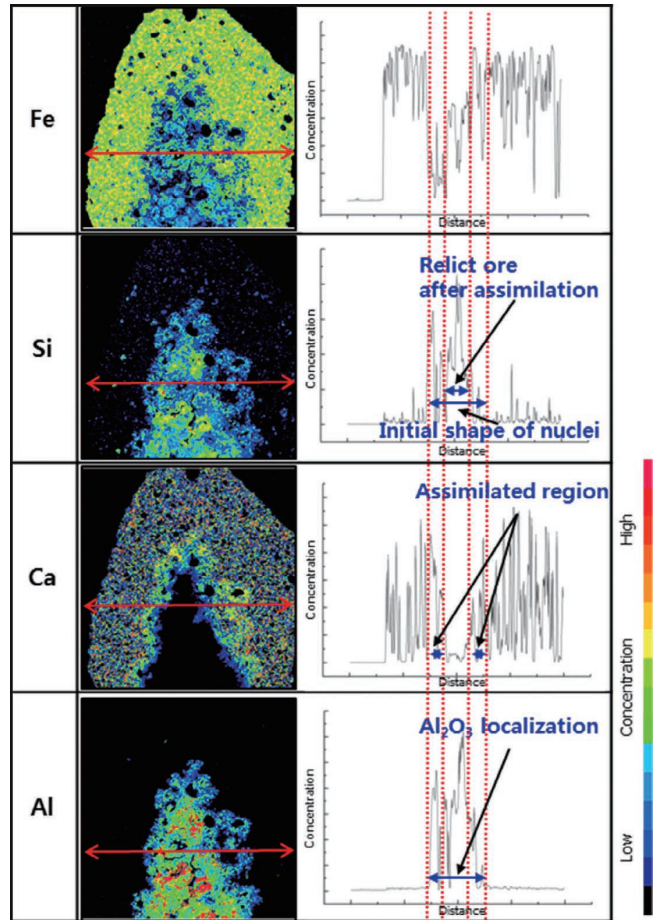**Fig. 8.** EPMA area and line mapping of Fe, Si, Ca and Al for A-N sample.

Fig. 9. EPMA area and line mapping of Fe, Si, Ca and Al for A-J sample.

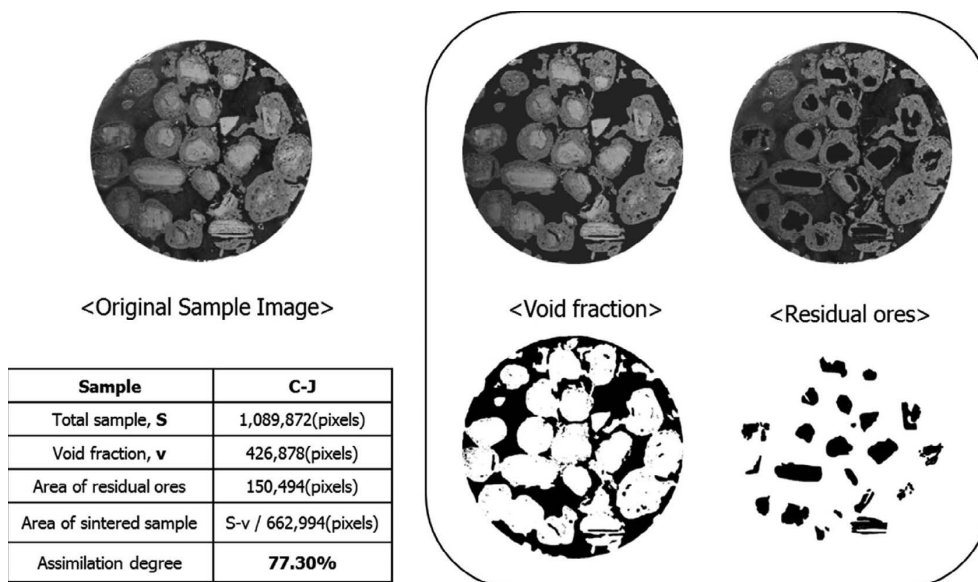| Sample	C-J
Total sample, **S**	1,089,872(pixels)
Void fraction, **v**	426,878(pixels)
Area of residual ores	150,494(pixels)
Area of sintered sample	S-v / 662,994(pixels)
Assimilation degree	**77.30%**

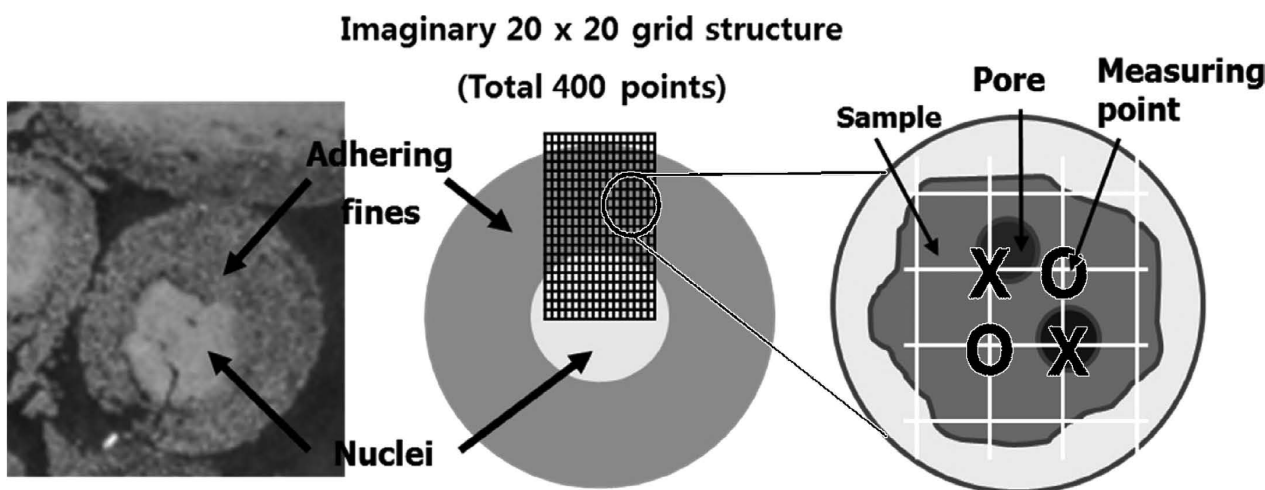**Fig. 3.** An example calculation of determining the assimilation degree (C-J sample).

Fig. 4. EPMA sweeping area analysis method.

sample contains same amount of coke breeze. The oxidation effect of magnetite on sintering temperature was ignored because the melt formation at adhering fines may limit the oxidation of magnetite. The tumble strength and reducibility were evaluated for the sintered samples. In the present study, due to the limited quantity of tested sample, the standard test methods for tumble strength (ISO 2171) and reducibility (ISO 8176) were modified so that they could be applied to smaller amount of sintered sample. That is, 100 and 1.5 g of sintered samples were tested for tumble strength and reducibility, respectively.

3. Results and Discussion

3.1. Assimilation Degree of Quasi-Particles

The assimilation starts with the formation of melt at the adhering fines, and subsequently the melt reacts with the nuclei. The melt property plays an important role in determining the assimilative characteristics and final sinter quality.[10,13] **Figure 5** shows the measured assimilation degrees of the quasi-particle samples. The C-N and A-N samples showed

$$Assimilation\ degree(\%) = \left(1 - \frac{area\ of\ residual\ ores}{area\ of\ sintered\ sample}\right) \times 100$$
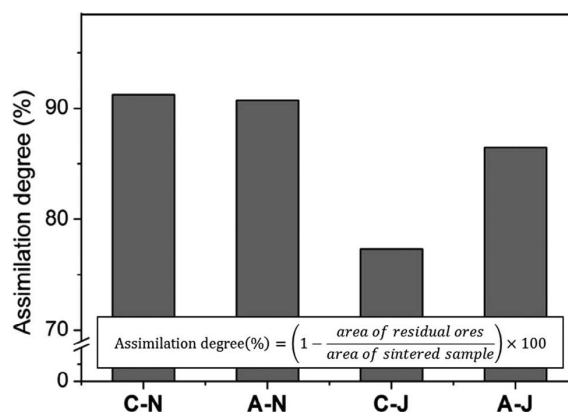
Fig. 5. Measured assimilation degree of quasi-particle samples from image analysis.

higher assimilation degree than those of C-J and A-J samples. This result would be ascribed to the adhering fines comprising quasi-particle. It is commonly known that magnetite is less reactive and has poor characteristics in the melt formation compared with hematite.[14,15] Therefore, lower

assimilation degree was obtained for the samples comprising ultra-fine magnetite ore J (C-J and A-J) compared with the samples comprising ultra-fine hematite ore N (C-N and A-N). In order to explain the assimilation behavior of quasi-particles, the microstructure analyses were conducted for A-N and A-J samples particularly.

3.2. Assimilation Behavior of Quasi-Particles Interpreted by Microstructure Analysis

The quasi-particle structures after assimilation are presented in **Figs. 6** and **7** for the A-N and A-J samples, respectively. Large number of micro and macro pores was observed at the sintered region in A-N sample as shown in Fig. 6(a). Since the assimilation of quasi-particle takes place by the interaction between nuclei and the melt formed in the adhering fines, it is believed that the viscosity of melt is one of the key factors to determine the final pore structure. In case the ultra-fine hematite ore N was used as adhering fines of quasi-particle, the melt of calcium ferrite with low viscosity might initially be produced, which makes contribution to the formation of the porous structure in A-N sample. The irregular shape of pores might be ascribed to the increase in the melt viscosity, which resulted from the dissolution of Al_2O_3 and SiO_2 in Ore A into the assimilated region in the progress of assimilation. Therefore, higher assimilation of nuclei and adhering fines was observed in A-N sample.

On the other hand, in the case of A-J sample, limited number of pores and dense structure were observed in the region of adhering fines as shown in Fig. 7(a). Since magnetite is thought to be less reactive than hematite and calcium ferrite melt cannot be formed directly from the magnetite, it

was expected that magnetite has poor characteristics of melt formation, which limits the assimilation.[14,15] When the ultra-fine magnetite ore J was used as adhering fines of quasi-particle, limited formation of calcium ferrite melt with low viscosity was expected. Therefore, the assimilation of nuclei and adhering fines was observed only in the narrower region with the formation of 'interfacial layer' of silicate as shown in Fig. 7(b). Figures 6(c) and 7(c) clearly shows the different melt formation behaviors of ore N and J in the regions of adhering fines, respectively. The formation of large amount of calcium ferrite indicates that the calcium ferrite melt was easily produced for the case of hematite ore N, while formation of the network of fused magnetite-magnetite grain boundaries implies the limited generation of calcium ferrite melt for the magnetite ore J.[14]

To further investigate the different assimilation behaviors of A-N and A-J samples, EPMA mapping analysis was carried out for the elements of Fe, Al, Si and Ca. Since most of Si was initially located in the nuclei ore, the initial shape of nuclei could be identified by the distribution of Si concentration. The relict ore which did not react with the melt in the progress of assimilation could be identified from the absence of Ca distribution. In the case of A-N sample, as shown in **Fig. 8**, high concentration of Al was observed in the goethite region of nuclei. In addition, little amount of Al was distributed throughout the entire region of quasi-particle, which indicates that some of Al_2O_3 diffused out from the nuclei to the region of adhering fines in the progress of assimilation. Consequently, the A-N sample showed low extent of Al_2O_3 localization due to the high assimilation behavior. On the other hand, in the case of A-J sample, it was observed that Al was localized only in the nuclei region
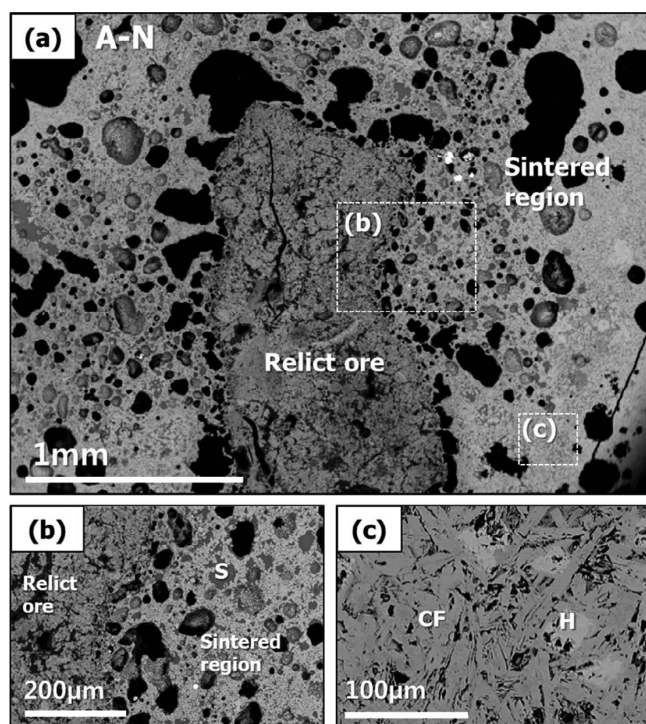

Fig. 6. Backscattered electron images of A-N sample. (a) Microstructure of a sintered quasi-particle. (b) Interface between relict ore and sintered region. (c) Adhering fines region. H: hematite, CF: calcium ferrite, S: silicate.
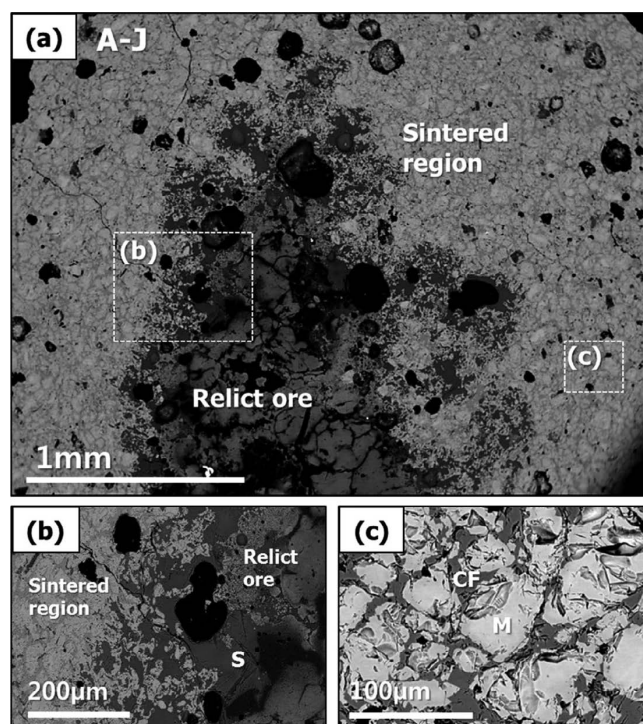

Fig. 7. Backscattered electron images of A-J sample. (a) Microstructure of a sintered quasi-particle. (b) Interface between relict ore and sintered region. (c) Adhering fines region. M: magnetite, CF: calcium ferrite, S: silicate.

as shown in **Fig. 9**. It is believed that the high extent of Al₂O₃ localization in A-J sample was resulted from the limited assimilation behavior. In addition, it appears that the localization of Al₂O₃ is affected by the formation of 'interfacial layer' between nuclei and adhering fines, which block the diffusion of Al₂O₃.

In particular, the distribution of Ca provides some remarkable differences in the assimilation behaviors between A-N and A-J. In the case of A-N, the concentration of Ca was gradually decreased from the adhering fines region to relict ore. It suggests that the calcium ferrite melt which formed at the adhering fines has large reactivity with nuclei (especially at the dehydrated goethite region), resulting in the high assimilation in A-N. On the other hand, in the case of A-J, the rapid decrease in Ca concentration was observed across the interfacial layer into the nucleus. This might indicate that the interaction between melt and nuclei was suppressed, which results in the limited assimilation of A-J.

3.3. Assimilation Behavior of Quasi-Particles Interpreted by EPMA Sweeping Area Analysis

For in-depth investigation on phase compositions by focusing on a single quasi-particle, EPMA sweeping area analysis was conducted, which will facilitate the understanding of the assimilation behavior of the samples. The analysis results were plotted on the CaO–SiO₂–Fe₂O₃ ternary diagram as shown in **Fig. 10**. Figure 10(c) provides two domains of melting point below 1 250°C indicated as domains α and β.[16] Since the primary fields of 3CaO·Fe₂O₃·3SiO₂ and CaO·Fe₂O₃ were located in domain α and β, respectively as indicated in Fig. 10(c), the primary phases producing initial melts were assumed to be 3CaO·Fe₂O₃·3SiO₂ domain α and CaO·Fe₂O₃ for domain β. In the case of A-N in Fig. 10(a), it was found that the distribution of chemical compositions was closely related to the domain β. This result might indicate that the calcium ferrite melt was initiated at the adhering fines and mainly participated in the assimilation of A-N. On the other hand, in the case of A-J in Fig. 10(b), high concentration of chemical compositions was found along the line connecting the composition of 3CaO·Fe₂O₃·3SiO₂ and Fe₂O₃, which represents the compositions of 'interfacial layer' between nuclei and adhering fines of A-J. This result

suggests that the initial melt probably formed with the composition of 3CaO·Fe₂O₃·3SiO₂ and the composition of melt moved to the Fe₂O₃ side in the progress of assimilation.

The assimilation behaviors of quasi-particles can be explained on the basis of penetration phenomena derived by capillary pressure. The Washburn equation expresses the kinetics of penetration as follows:[17,18]

$$v = \frac{dh}{dt} = \frac{r\gamma cos\theta}{4\eta h} \qquad (2)$$

where v: rate of entry into a horizontal capillary,
  h: the length of the liquid column (*i.e.* penetration length),
  t: penetration time,
  r: radius of capillary,
  γ: surface tension,
  θ: contact angle,
  η: viscosity of the liquid.

Integration of Eq. (2) with the boundary condition ($h=0$ and $t=0$) gives penetration length h by Eq. (3):

$$h = \left(\frac{r\gamma cos\theta}{2\eta} \right)^{1/2} \cdot t^{1/2} \qquad (3)$$

Equation (3) shows that the penetration length of melt depends on the both the nuclei property such as porosity (r) and melt properties such as surface tension (γ), contact angle (θ) and viscosity (η). In the present study, it was assumed that the nuclei property was constant since the identical nuclei ores were used for A-N and A-J. However, melt properties varies significantly depending on the composition and temperature. It indicates that the penetration behavior is essentially determined by the melt properties under some assumption that the nuclei property, penetration time and temperature are constant. Some available information was adopted from the literature to assess the impact of melt properties on the penetration behavior. The surface tensions were reported at 1 410°C with assumption of $\theta=0$ for Fe-saturated iron silicate melts with 0–34.98 wt% SiO₂ and Fe-saturated calcium ferrite melts with 1.76–26.90 wt% CaO in the range of 419–577 and 560–575 N·m⁻¹, respectively.[19] On the other hand, in the present study, the melt viscosities of initial compositions were estimated by using the thermodynamic calculation[16] as shown in **Fig. 11**. This
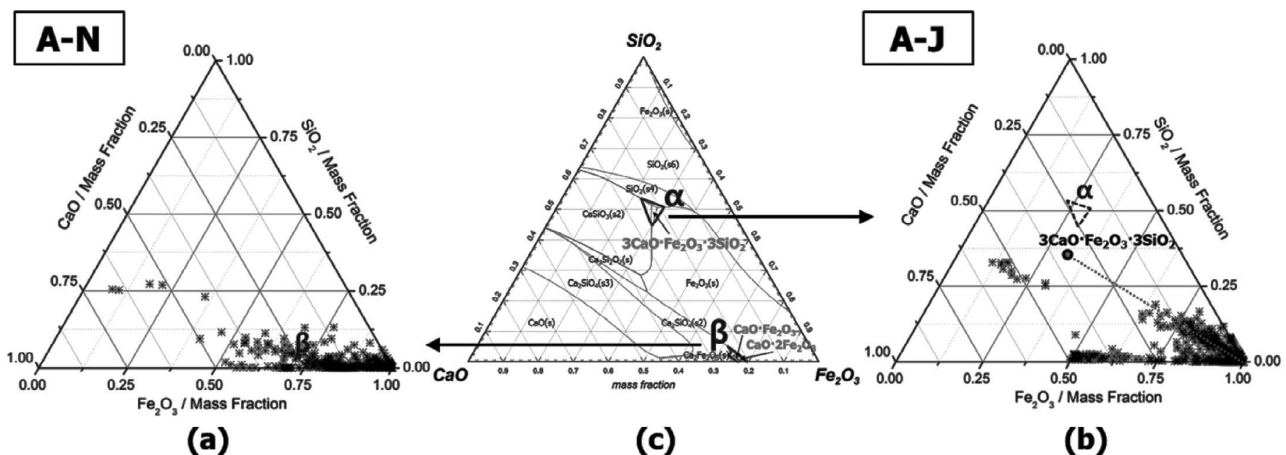

Fig. 10. Compositional distribution of (a) A-N and (b) A-J on CaO–SiO₂–Fe₂O₃ system with (c) melt regions below 1 250°C.

result showed that the viscosity of $3CaO \cdot Fe_2O_3 \cdot 3SiO_2$ has about 5 times higher than that of $CaO \cdot Fe_2O_3$ at 1 300°C. Since the penetration behavior is essentially determined by melt properties in terms of the ratio of surface tension to viscous force (*i.e.* $\gamma cos\theta / \eta$), the above discussion indicates that the assimilation behavior of primary melt is believed to dominantly be affected by the melt viscosity. Therefore, the lower assimilation degree of A-J can be explained by the higher viscosity of $3CaO \cdot Fe_2O_3 \cdot 3SiO_2$ melt.

From the above results, the assimilation mechanisms of A-N and A-J were summarized in **Fig. 12**. For the A-N sample which was comprised of high Al_2O_3 pisolitic ore A as nuclei and ultra-fine hematite ore N as adhering fines:

a) Calcium ferrite melt initially forms in the region of the adhering fines by the reaction of ultra-fine hematite N with CaO.

$$Fe_2O_3(s) + CaO(s) = CaO \cdot Fe_2O_3(s) \quad .... \quad (4)$$

$$\Delta G^\circ = -30\ 000 - 4.8T \ (J/mol)^{20)} \quad .... \quad (5)$$
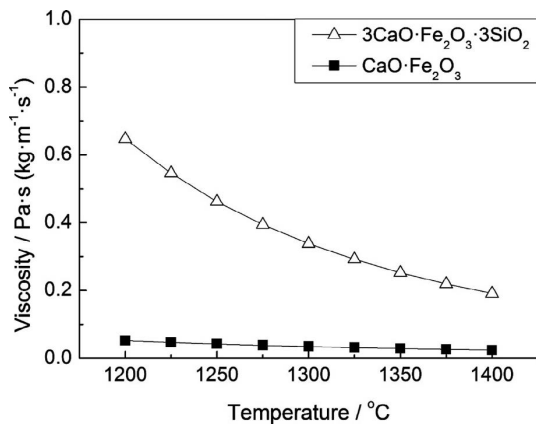
Fig. 11. Viscosity of $3CaO \cdot Fe_2O_3 \cdot 3SiO_2$ and $CaO \cdot Fe_2O_3$.

b) Assimilation starts with the penetration of calcium ferrite melt into the nuclei and then the melt with low viscosity reacts with dehydrated goethite of nuclei.

c) In the progress of assimilation, the viscosity of melt gradually increases as Al_2O_3 and SiO_2 of the nuclei dissolved into the melt.

d) Finally, granular hematite and silicate phases were precipitated upon cooling and Al_2O_3 were mainly localized in the assimilated region. However, due to the high fluidity of the melt, some amount of Al_2O_3 diffused out to the region of adhering fines.

On the other hand, for the A-J sample which was comprised of high Al_2O_3 pisolitic ore A as nuclei and ultra-fine magnetite ore J as adhering fines:

a) Since the calcium ferrite cannot be formed directly from magnetite,[14] it is expected that the melt of fayalite ($2FeO \cdot SiO_2$) preferentially forms at the interface between nuclei and adhering fines.

$$2FeO(s) + SiO_2(s) = 2FeO \cdot SiO_2(s) \quad .... \quad (6)$$

$$\Delta G^\circ = -36\ 200 - 21.1T \ (J/mol)^{21)} \quad .... \quad (7)$$

b) Subsequently, the fayalite melt reacts with CaO to generate the melt mainly comprising the composition of $3CaO \cdot Fe_2O_3 \cdot 3SiO_2$. This transformation could be interpreted based on the dependence Fe^{3+}/Fe^{2+} ratio on CaO content.[22] That is, the Fe^{3+}/Fe^{2+} ratio increased with increasing CaO content in the melt:

$$3(2FeO \cdot SiO_2) + 3CaO + \frac{3}{2}O_2$$
$$= 3CaO \cdot Fe_2O_3 \cdot 3SiO_2 + 2Fe_2O_3 \quad .... \quad (8)$$
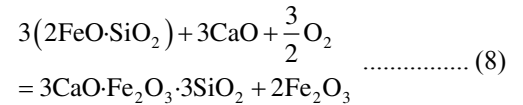
c) As a result of the high viscosity of $3CaO \cdot Fe_2O_3 \cdot 3SiO_2$ melt, the assimilation in A-J sample takes place only at the interface between nuclei and adhering fines by forming the interfacial layer with the compositions along the line from
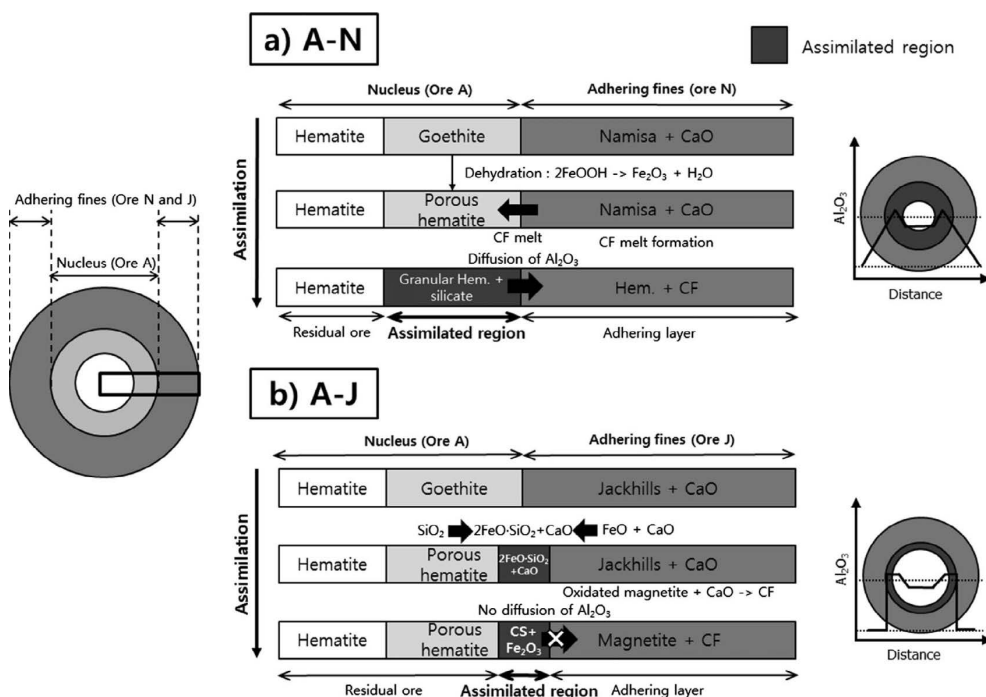

Fig. 12. Summary of assimilation mechanisms of (a) A-N and (b) A-J.

3CaO·Fe$_2$O$_3$·3SiO$_2$ to Fe$_2$O$_3$. The formation of interfacial layer could block the Al$_2$O$_3$ diffusion so that Al$_2$O$_3$ localized only in the nuclei region.

3.4. Evaluation of Sinter Quality

Small scale sintering test was carried out to evaluate the sinter quality of quasi-particle samples. **Figure 13** shows the effects of Al$_2$O$_3$ and SiO$_2$ content on the tumble strength and reducibility of the sample. A decrease of tumble strength and an increase of reducibility were found in the samples with nuclei of high Al$_2$O$_3$ pisolitic ore A compared with those of the samples with nuclei of dense hematite ore C. This result is in good agreement with the previous researches[2,6] about the detrimental effect of high Al$_2$O$_3$ on tumble strength. Furthermore, regardless of the nuclei ores, lower tumble strength and higher reducibility were observed in the samples with adhering fines of ultra-fine hematite ore compared with that of the samples with adhering fines of ultra-fine magnetite ore.

In particular, the A-J sample showed reasonable sinter quality from viewpoints of the compromise between the tumble strength and reducibility. The sinter quality of A-J sample was similar to that of C-N sample which is considered a suitable sinter sample in the present work. However, in the case of A-N sample, it is probably not suitable for the sinter sample due to the low tumble strength even though it has the highest reducibility. Consequently, it can be conclud-ed that the ultra-fine magnetite ore J is more suitable adhering fines than ultra-fine hematite ore N in terms of sinter quality.

4. Conclusions

The assimilation behavior of quasi-particle was investigated to utilize the high Al$_2$O$_3$ pisolitic ore as nuclei of quasi-particle. From the findings, the following conclusions were obtained.

(1) In case the ultra-fine hematite ore was used as adhering fines of quasi-particle, CaO·Fe$_2$O$_3$ melt with low viscosity was predominantly participated in the assimilation. Due to the porous structure and low extent of Al$_2$O$_3$ localization, the detrimental effect of Al$_2$O$_3$ on the strength of quasi-particle was not fully controlled.

(2) When the ultra-fine magnetite ore was employed as adhering fines of quasi-particle, 3CaO·Fe$_2$O$_3$·3SiO$_2$ melt with high viscosity was predominantly participated in assimilation. As a result, the assimilation was suppressed by the formation of 'interfacial layer' along the line connecting the compositions of 3CaO·Fe$_2$O$_3$·3SiO$_2$ and Fe$_2$O$_3$ in CaO–SiO$_2$–Fe$_2$O$_3$ ternary system. Due to the dense structure and high extent of Al$_2$O$_3$ localization, the detrimental effect of Al$_2$O$_3$ on the strength was reasonably controlled.

(3) The quasi-particle comprising high Al$_2$O$_3$ pisolitic ore and ultra-fine magnetite ore showed competitive sinter quality similar to the quasi-particle sample consisting nuclei of dense hematite and adhering fines of ultra-fine hematite, resulting in the high sinter quality.

Fig. 13. Effect of Al$_2$O$_3$ and SiO$_2$ content in the ores on the (a) tumble strength and (b) reducibility of quasi-particle samples.

REFERENCES

1) S. W. Kim, Y. K. Ji and I. K. Suh: *POSCO Res. Paper*, **18** (2013), 1.
2) L. Lu, R. J. Holmes and J. R. Manuel: *ISIJ Int.*, **47** (2007), 349.
3) C. E. Loo: *ISIJ Int.*, **45** (2005), 436.
4) L. Hsieh: *ISIJ Int.*, **45** (2005), 551.
5) J. Okazaki and K. Higuchi: *ISIJ Int.*, **45** (2005), 427.
6) S. Machida, K. Nushiro, K. Ichikawa, H. Noda and H. Sakai: *ISIJ Int.*, **45** (2005), 513.
7) X. LV, C. Bai, Q. Deng, X. Huang and G. Qiu: *ISIJ Int.*, **51** (2011), 722.
8) T. Otomo, Y. Takasaki and T. Kawaguchi: *ISIJ Int.*, **45** (2005), 532.
9) N. Oyama, T. Higuchi, S. Machida, H. Sato and K. Takeda: *ISIJ Int.*, **49** (2009), 650.
10) D. Debrincat, C. E. Loo and M. F. Hutchens: *ISIJ Int.*, **44** (2004), 1308.
11) Z. Wang, K. Ishii, Y. Sasaki and T. Tsutsumi: *Tetsu-to-Hagané*, **84** (1998), 689.
12) Z. Wang, Y. Sasaki, Y. Kashiwaya and K. Ishii: *Tetsu-to-Hagané*, **86** (2000), 370.
13) L. X. Yang and L. Davis: *ISIJ Int.*, **39** (1999), 239.
14) J. M. F. Clout and J. R. Manuel: *Powder Technol.*, **130** (2003), 393.
15) L. X. Yang and D. Witchard: *ISIJ Int.*, **38** (1998), 1069.
16) C. W. Bale, E. Bélisle, P. Chartrand, S. A. Decterov, G. Eriksson, K. Hack, I.-H. Jung, Y.-B. Kang, J. Melançon, A. D. Pelton, C. Robelin and S. Petersen: *Calphad*, **33** (2009), 295.
17) C. E. Loo and L. T. Matthews: *Trans. Inst. Min. Metall. C*, **101** (1992), 105.
18) J. Okazaki, K. Higuchi, Y. Hosotani and K. Shinagawa: *ISIJ Int.*, **43** (2003), 1384.
19) M. Kidd and D. R. Gaskell: *Metall. Trans. B*, **17B** (1986), 771.
20) H. G. Lee: Chemical Thermodynamics for Metals and Materials, Imperial College Press, London, (1999), 286.
21) R. J. Fruehan: The Making, Shaping and Treating of Steel, Steelmaking and Refining Volume, 11th ed., AISE Steel Foundation, Pittsburgh, PA, (1998), 20.
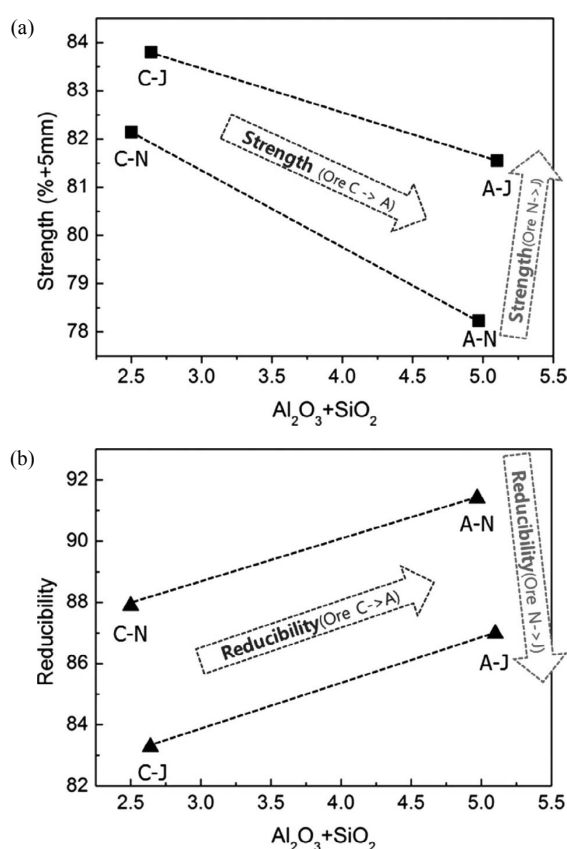22) L. Yang and G. R. Belton: *Metall. Mater. Trans. B*, **29B** (1998), 837.